Charge transfer between S^{2+} and He: A comparative study of quantal and semiclassical approaches

L. B. Zhao* and P. C. Stancil†
Department of Physics and Astronomy and the Center for Simulational Physics, University of Georgia, Athens, Georgia 30602-2451, USA

J.-P. Gu, G. Hirsch,‡ and R. J. Buenker§
Fachbereich C-Mathematik und Naturwissenschaften, Bergische Universität Wuppertal, D-42097 Wuppertal, Germany

T. W. Imai and M. Kimura‖
Graduate School of Sciences, Kyushu University, Fukuoka 812-8581, Japan
(Received 21 June 2005; published 19 September 2005)

A comparative study of charge transfer in collisions of ground-state S^{2+} ions with He has been performed within fully quantal and semiclassical molecular-orbit close-coupling approaches. The processes for capture into $S^+(^4S^0, ^2D^0, ^2P^0)+He^+$ are taken into account. Quantal and semiclassical cross sections were evaluated, respectively, in the diabatic and adiabatic representations and found to be in good agreement. The calculations show that at collision energies below about 40 eV/u, the charge-transfer processes are dominated by $S^{2+}(^3P)+He \rightarrow S^+(^2D^0)+He^+$, and capture into the $^2P^0$ and $^4S^0$ states becomes comparable with that into the $^2D^0$ state above 40 eV/u and 600 eV/u, respectively. The multireference single- and double-excitation configuration-interaction method was utilized to obtain adiabatic potentials and nonadiabatic coupling matrix elements. A detailed comparison of quantal and semiclassical transition probabilities is discussed. State-selective and total rate coefficients are presented with temperatures between 10 000 K and 5.0×10^6 K.

DOI: 10.1103/PhysRevA.72.032719 PACS number(s): 34.10.+x, 34.20.Mq, 34.70.+e

I. INTRODUCTION

Charge transfer is one of the most important atomic processes in collisions of ions with atoms, molecules, and surfaces. Investigations of charge transfer, or electron capture, are involved in many practical applications in fields such as astrophysics, controlled fusion plasmas, radiology, and thin-film maufacturing. Depending on physical conditions, the charge-transfer reaction may dominantly influence the ionization balance in astronomical and laboratory plasmas and may significantly contribute to ion emission spectra by populating excited states. The produced line emission can be utilized to diagnose the composition and properties of terrestrial and nonterresterial plasmas, such as comets [1], planetary nebulae, and supernova remnants [2,3]. In medicine application, a so-called radiation therapy was developed to cure tumors. The treatment takes effect by charge transfer between bombarding ions and biomolecules in human cells and therefore inducing destruction of cancerous cells.

During the past decades, intense experimental and theoretical efforts have been made towards understanding charge-transfer reactions. The measurement techniques have been progressly raised and the computational methods, such as the hyperspherical method [4], the common reaction coordinate method [5], and so on, have turned out to be successful. So far, studies of charge transfer for a variety of ion-atom and ion-molecule systems have been published (see, e.g., [6]). However, to the best of our knowledge, electron capture for collisions of S^{2+} ions with He has not yet been reported. Recently, Shang *et al.* [7] have developed a thermal-chemical model to describe the accretion disks of young stellar objects and to predict the strengths of forbidden emission lines. They considered the $^2D^0_{3/2} \rightarrow {}^4S^0$ (6731 Å) and $^2D^0_{5/2} \rightarrow {}^4S^0$ (6716 Å) transitions of S II and the 6300-Å line of O I. The 6717/6731 and 6731/6300 line ratios are diagnostics of electron density and temperature, respectively. In their model, the charge exchange of O^+ with H and its reverse are included to determine the oxygen ionization fraction, and all sulfur was assumed to be singly ionized. As S^+ can be produced by electron capture in collisions of S^{2+} with He, it is important to provide accurate charge-transfer cross sections for the $S^{2+}+He \rightarrow S^+ + He^+$ process for a wide range of collision energies. Furthermore, S II transitions were observed in H II regions [8], Seytert galaxies [9], and planetary nebulae [10].

Besides the practical importance mentioned above, investigations of charge transfer for ion-atom and ion-molecule collisions are also of fundmental physics interest. For example, it is very interesting to obtain information on molecular structures and interactions in ion-atom or ion-molecule systems. Some features which it is difficult to calculate directly, such as potentials and couplings in the interior region of small internuclear distances, may be explored by comparing measured and evaluated cross sections. The comparisons are also useful to check the validity of classical and semi-

*Electronic address: zhao@physast.uga.edu
†Electronic address: stancil@physast.uga.edu
‡Deceased.
§Electronic address: buenker@uni-wuppertal.de
‖Electronic address: mineoscc@mbox.nc.kyushu-u.ac.jp

classical theories describing the collision systems [11]. Recently, we found significant discrepancies between fully quantal and semiclassical capture cross sections for collisions of O^+ with He [12] and of N with H^+ [13]. Fully quantal and semiclassical molecular-orbital close-coupling (QMOCC and SCMOCC) approaches are expected to agree if collision energies are not too low ($E > 10$ eV/u). For examples, it has been shown that quantal and semiclassical charge-transfer cross sections or probabilities in collisions of Be^{4+} with H [5], C^{2+} with He [14], and S with H^+ [15] are in good agreement for high collision energies. The existing discrepancies for the OHe^+ and NH^+ systems stimulated us to carry out a comparative study of electron capture in S^{2+} + He collisions with the QMOCC and SCMOCC approaches. In the present paper, the concerned charge-transfer reactions are

$$S^{2+}(^3P) + \mathrm{He} \rightarrow \mathrm{S}^+(^4S^0, ^2D^0, ^2P^0) + \mathrm{He}^+ - \Delta E. \qquad (1)$$

In the next section, we describe calculations of the molecular potentials and nonadiabatic radial and rotational coupling matrix elements the SHe^{2+} system. Section III briefly surveys the QMOCC and SCMOCC approaches. In Sec. IV, total and state-selective cross sections and rate coefficients are presented and the QMOCC and SCMOCC results are compared. Section V summarizes the main results. Atomic units are used thoughout unless otherwise noted.

II. ELECTRONIC STRUCTURE CALCULATIONS

The adiabatic potential energy curves and nonadiabatic radial and rotational coupling matrix elements are obtained with the *ab initio* multireference single- and double-excitation configuration-interaction (MRD-CI) method, with configuration selection and energy extrapolation. The MRD-CI method and its application to some molecular systems have been reported by Buenker and co-workers (see, e.g., [16–18]). The details of the method can be found in their papers. Here we give only a very brief summary. The helium atomic (Gaussian) orbital basis set is the same as in our previous study [19] with a slight modification characterized as $(9s4p1d)/[7s3p1d]$. For the sulfur atom, the frozen-core approximation is used for $1s$, $2s$, and $2p$ electrons and the $(12s9p)$ basis was contracted into $[6s5p]$ and augmented with two d and f polarization functions. The exponents for s-, p-, and d-type Rydberg functions have been reoptimized to give 0.023, 0.020, and 0.015, respectively. The final contracted basis set was taken to be $[7s6p3d1f]$. The potentials of the initial molecular states formed by $S^{2+}(^3P)$ + He and the final states by $S^+(^4S^0, ^2D^0, ^2P^0)$ + He^+ and radial and rotational couplings among these states were calculated from the internuclear distance $R = 2.0$ to $R = 20.0$ a.u.

As we consider collisions of the ground-state S^{2+} ions with He and neglect transitions due to spin-orbit interactions, only triplet molecular states are involved. The seven adiabatic potential curves are plotted as a function of R in Fig. 1. The two electronic states $1\ ^3\Sigma^-$ and $1\ ^3\Pi$ are formed in the approach of $S^{2+}(3p^2\ ^3P)$ with He, the state $2\ ^3\Sigma^-$ by $S^+(3p^3\ ^4S^0)$ with He^+, the three states $2\ ^3\Pi$, $1\ ^3\Delta$, and $3\ ^3\Sigma^-$

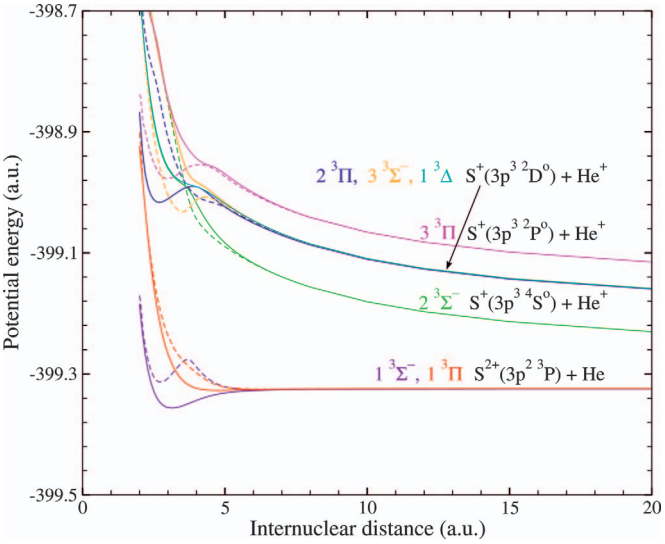

FIG. 1. (Color) The adiabatic (solid lines) and diagonal diabatic (dashed lines) potential energies for the SHe^{2+} system as a function of internuclear distance R.

by $S^+(3p^3\ ^2D^0)$ with He^+, and the state $3\ ^3\Pi$ by $S^+(3p^3\ ^2P^0)$ with He^+. It should be mentioned that electron capture into $1\ ^3\Sigma^+$ formed by $S^+(3p^3\ ^2P^0)$ with He^+ is omitted since its contribution is expected to be small. Thus only transitions from the $1\ ^3\Sigma^-$ and $1\ ^3\Pi$ states into the $2\ ^3\Sigma^-$, $2\ ^3\Pi$, $1\ ^3\Delta$, $3\ ^3\Sigma^-$, and $3\ ^3\Pi$ states are taken into account. The calculated MRD-CI asymptotic energies are presented for the seven molecular states relative to the $S^+(3p^3\ ^2P^0)$ + He^+ channel and compared with available theoretical [20] and experimental energies [21,22] in Table I. Good agreement is seen with Refs. [20–22]. The maximium relative error of the current results from the experimental data is less than 3%.

The nonadiabatic radial couplings are plotted as a function of R in Fig. 2. Three strong peaks occur at $R = 2.10$, 3.76, and 4.10 a.u. They correspond to the couplings $1\ ^3\Pi$-$2\ ^3\Pi$, $2\ ^3\Sigma^-$-$3\ ^3\Sigma^-$, and $2\ ^3\Pi$-$3\ ^3\Pi$, respectively. These couplings may significantly contribute to the charge-transfer processes in Eq. (1). Amezian and Bacchus-Montabonel [20] reported calculations of the radial $1\ ^3\Pi$-$2\ ^3\Pi$ and $2\ ^3\Pi$-$3\ ^3\Pi$ couplings. We found good agreement between the current MRD-CI matrix elements and those of Amezian and Bacchus-Montabonel. In Fig. 3, the rotational couplings are displayed. These couplings drive transitions between states of different spatial symmetry. The potentials have been transformed from the adiabatic representation to the diabatic representation using Eqs. (4)–(6) (see Sec. III for details). The transformed potentials are required for the QMOCC calculations. The diagonal diabatic potential energies (dashed curves) are displayed in Fig. 1, and the off-diagonal matrix elements U_{ij} are illustrated in Fig. 4, where the order of the molecular states is $1\ ^3\Sigma^-$, $1\ ^3\Pi$, $2\ ^3\Sigma^-$, $2\ ^3\Pi$, $3\ ^3\Sigma^-$, $1\ ^3\Delta$, and $3\ ^3\Pi$, corresponding to the asymptotic adiabatic labeling. The U_{61}, U_{63}, and U_{65} are zero, as the couplings between $^3\Delta$ and $^3\Sigma^-$ are zero.

Beyond $R = 20.0$ a.u., the potentials for the entrance channels are described by the charge-induced-dipole interactions

TABLE I. Comparison of asymptotic separated-atom energies in eV between the MRD-CI calculations and experiments for the seven lowest triplet molecular states of SHe^{2+}. These states are of symmetries $^3\Sigma^-$, $^3\Pi$, and $^3\Delta$.

Asymptotic atomic state	Mol. state	This work	Theory[a]	Expt.[b]	Expt.[c]
$S^{2+}(3s^2 3p^2\ ^3P)+He$	$1\ ^3\Sigma^-$	0.000			0.000
	$1\ ^3\Pi$	0.016	0.000	0.000	—
$S^{+}(3s^2 3p^3\ ^4S^o)+He^+$	$2\ ^3\Sigma^-$	1.214			1.179
$S^{+}(3s^2 3p^3\ ^2D^o)+He^+$	$2\ ^3\Pi$	3.131	3.075	3.047	3.024
	$1\ ^3\Delta$	3.156			—
	$3\ ^3\Sigma^-$	3.158			—
$S^{+}(3s^2 3p^3\ ^2P^o)+He^+$	$3\ ^3\Pi$	4.244	4.217	4.245	4.224

[a]Amezian and Bacchus-Montabonel [20].
[b]Bashkin and Stoner [21].
[c]NIST Atomic Spectra Database [22].

$$V_L(R) = -\frac{\alpha_d}{2R^4} + E_\infty, \tag{2}$$

where α_d is the dipole polarizability of the neutral He atoms and E_∞ is the separated-atom energy. All the quantities in Eq. (2) are in atomic units (a.u.). For the exit channels, the long-range potentials ($R > 20.0$ a.u.) are Coulombic. E_∞ is determined using these parameters and the *ab initio* potentials.

III. SCATTERING THEORY

The quantal and semiclassical molecular-orbital close-coupling approaches to describe charge transfer in ion-atom collisions have been formulated by Zygelman *et al.* (QMOCC) [23] and by Kimura and Lane (SCMOCC) [6]. Here we only give brief summaries of these two approaches.

A. Quantal approach

In the diabatic representation, a coupled set of molecular-orbital close-coupling equations is written as

$$-\frac{1}{2\mu}\nabla^2 G(\mathbf{R}) + U(R)G(\mathbf{R}) = EG(\mathbf{R}), \tag{3}$$

where μ is the nuclear reduced mass of the ion-atom pair, E is the relative collision energy in the center-of-mass frame, $\mathbf{R}$ is the coordinate of the relative nuclear motion, $G(\mathbf{R})$ is the scattering amplitude describing relative motion of the nuclei, and $U(R)$ with $R=|\mathbf{R}|$ is the diabatic potential matrix whose off-diagonal elements are responsible for driving charge transfer in the diabatic representation, defined by

$$U(R) = W(R)[V(R) - P(R)]W^{-1}(R), \tag{4}$$

where $V(R)$ is a diagonal matrix with elements consisting of adiabatic eigenvalues for each channel state, $W(R)$ is the unitary matrix that obeys the equation

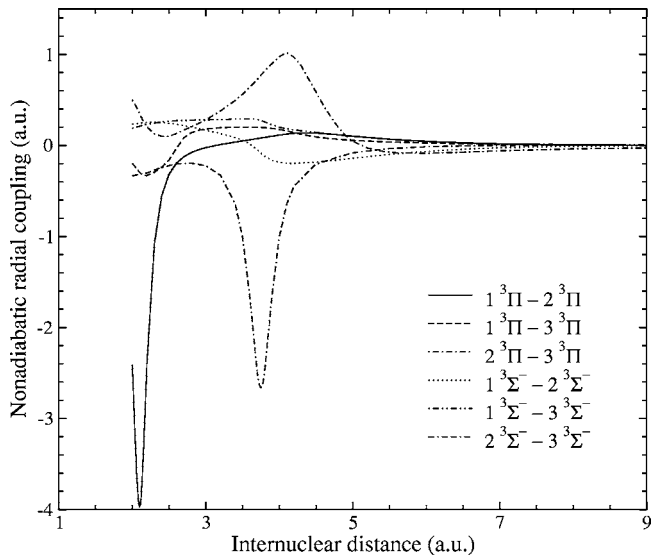

FIG. 2. The nonadiabatic radial couplings for the SHe^{2+} system as a function of internuclear distance R.

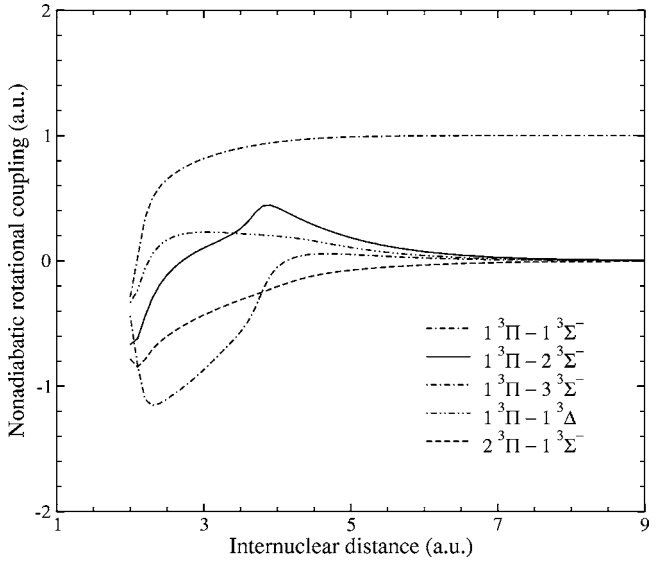

FIG. 3. The nonadiabatic rotational couplings for the SHe^{2+} system as a function of internuclear distance R.

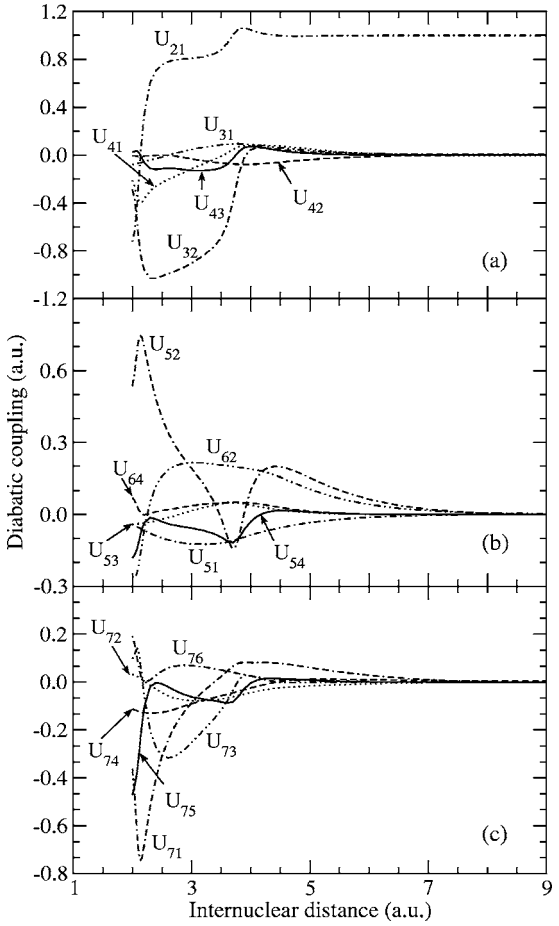

FIG. 4. The off-diagonal diabatic potentials for the SHe^{2+} system as a function of internuclear distance R.

$$\frac{dW(R)}{dR} + iW(R)A^{rad}(R) = 0, \tag{5}$$

and $P(\mathrm{R})$ is a coupling matrix whose elements are given by [24,25]

$$P_{\alpha\beta} = \mp \frac{1}{\mu R^2}[(J \mp \Lambda_\alpha)(J \pm \Lambda_\alpha + 1)]^{1/2} A^{rot}_{\alpha\beta}\delta(\Lambda_\alpha, \Lambda_\beta \mp 1), \tag{6}$$

where J is the total angular momentum, Λ is the component of electronic angular momenta along the internuclear axis, and $A^{rad}(R)$ and $A^{rot}(R)$ are, respectively, the radial and rotational components of the vector potential $[A(\mathbf{R})]_{\alpha\beta} = i\langle\psi_\alpha|\nabla_{\mathbf{R}}|\psi_\beta\rangle$, with ψ_α and ψ_β being the adiabatic electronic eigenfunctions.

By introducing a partial-wave decomposition for $G(\mathbf{R})$, Eq. (3) can be further simplified. The resulting set of radial coupled equations may be solved with the log-derivative method of Johnson [26]. From the numerical results of the log-derivative and asymptotic expressions of the radial functions, the K matrix may be extracted and thus the scattering matrix S is obtained:

$$S_J = [I + iK_J]^{-1}[I - iK_J]. \tag{7}$$

Finally the charge-transfer cross sections from channel α to channel β is expressed in terms of the scattering matrix elements

$$\sigma_{\alpha\to\beta} = \frac{\pi g_\alpha}{k_\alpha^2}\sum_J (2J+1)|(S_J)_{\alpha\beta}|^2, \tag{8}$$

where k_α denotes the wave number for center-of-mass motion of the initial ion-atom channel and g_α is an approach probability factor of the initial channel α. Electron translation factors (ETF's—e.g., [6]) are not included in the current calculations, since the influence of ETF's is expected to be important for $E > 1$ keV/u (e.g., [27,28]). Our results may be uncertain above this energy, but probably by no more than 50%.

B. Semiclassical approach

In the adiabatic representation, the total wave function for a collision system is expanded in terms of time-dependent coefficients $a(t)$ and electronic basis functions with atomic-type ETF's. Substituting the total wave function into the time-dependent Schrödinger equation and retaining the ETF correction up to the first order of the ion-atom relative velocity v, one arrives at a set of first-order coupled differential equations [6,29], given in matrix notation,

$$i\frac{da(t)}{dt} = [\varepsilon + \mathbf{v}\cdot(\mathbf{A} + \mathbf{C})]a(t), \tag{9}$$

where ε is the Born-Oppenheimer potential energy matrix, $\mathbf{A}$ represents the nonadiabatic coupling matrix, and $\mathbf{C}$ is the ETF correction of $\mathbf{A}$ (to first order in v). We note the notation here is different from that adopted in Refs. [6,29]. We assume a classical straight-line trajectory for the heavy-particle motion. By numerically solving the coupled equations (9), the expansion coefficient $a(t)$ is obtained. Thus the transition probabilities from an initial state i to a final state f, defined as a function of impact parameter b at $t \to +\infty$, is

$$\mathcal{P}_{if}(b) = |a(t \to +\infty; b)|^2. \tag{10}$$

The charge-transfer cross sections are determined by integrating the partial sublevel cross sections $\sigma_{if}(b)$ over all impact parameters:

$$\sigma_{if} = \int_0^\infty \sigma_{if}(b)db = 2\pi\int_0^\infty b\mathcal{P}_{if}(b)db. \tag{11}$$

Kimura and Lane showed schematically the relation of the fully quantal and semiclassical approaches in Ref. [6]. It is readily observed that in these two approaches, both molecular electronic motions are described quantum mechanically, while the motion of heavy nuclei is treated quantum mechanically and classically, respectively. Thus one can utilize the same nonadiabatic radial and rotational couplings, which drive transitions between molecular states, for the QMOCC and SCMOCC calculations. The SCMOCC approach is quantitatively reliable if collision energies are not extremely

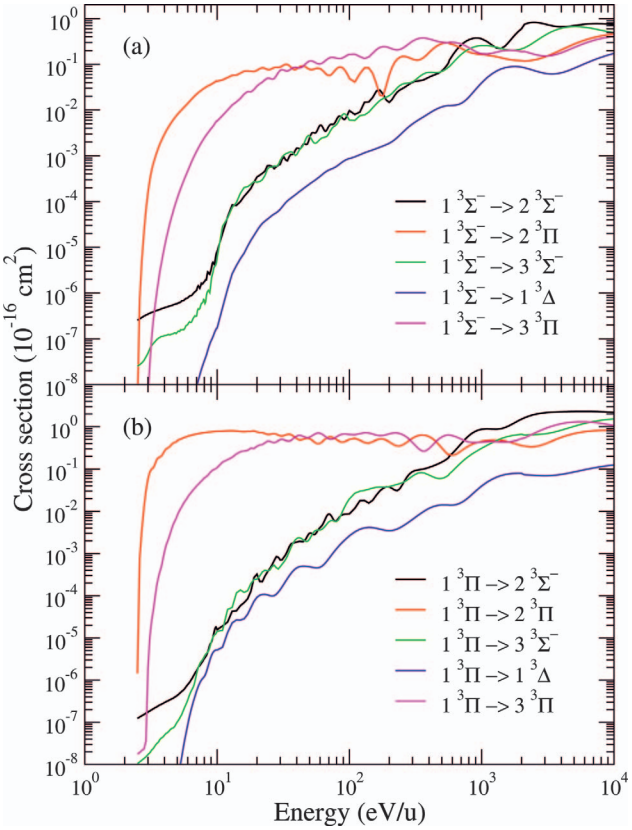

FIG. 5. (Color) State-to-state QMOCC charge-transfer cross sections due to S^{2+}+He collisions as a function of relative collision energy E. (a) and (b) represent transitions from the initial states $1\,^3\Sigma^-$ and $1\,^3\Pi$ of $S^{2+}(^3P)$, respectively, to the five final states of $S^+(^4S^0, ^2D^0, ^2P^0)$.

low. This is because in this situation the de Broglie wavelength of the relative motion of the nuclei is small compared with atomic dimensions.

The quantal and semiclassical transition probabilities can be compared in detail by taking $b=J/k$.

IV. RESULTS AND DISCUSSION

The quantal seven-channel close-coupling calculations were performed using the electronic structure and coupling data in Sec. II. The relative collision energy considered ranges from 2.5 eV/u to 10^4 eV/u. The contributions from the individual partial waves were summed as in Eq. (8) until a convergence of cross sections is achieved. The state-to-state cross sections for electron-capture processes $1\,^3\Sigma^-$, $1\,^3\Pi \rightarrow 2\,^3\Sigma^-$, $2\,^3\Pi$, $3\,^3\Sigma^-$, $1\,^3\Delta$, and $3\,^3\Pi$ are plotted in Fig. 5. The cross sections for the $1\,^3\Pi \rightarrow 2\,^3\Pi$ transition in Fig. 5(b) show a sudden drop at 3.0 eV/u, even though the threshold for the process occurs at 0.85 eV/u. This higher effective threshold results because the transition is driven by the $1\,^3\Pi$-$2\,^3\Pi$ radial coupling which peaks at $R=2.1$ a.u. (see Fig. 2). However, due to the repulsive nature of the $1\,^3\Pi$ at small R and the Coulombic behavior of the $2\,^3\Pi$, which asymptotically goes to $S^+(^2D^0)$+He^+, the corresponding avoided crossing occurs 0.4 hartree (3.0 eV/u) above the entrance channel (see Fig. 1). The coupling is not sampled for smaller collision energies. The $1\,^3\Pi$-$2\,^3\Pi$ coupling may enhance the other transitions by two-step processes. Figure 5(b) displays the strong $1\,^3\Pi \rightarrow 3\,^3\Pi$ transition. However, the larger cross sections do not stem from the direct $1\,^3\Pi \rightarrow 2\,^3\Pi$ coupling, because this coupling is very small (see Fig. 2). Instead, the $1\,^3\Pi \rightarrow 2\,^3\Pi$ followed by the $2\,^3\Pi \rightarrow 3\,^3\Pi$ is more effective. The other two transitions $1\,^3\Sigma^- \rightarrow 2\,^3\Pi$ and $1\,^3\Sigma^- \rightarrow 3\,^3\Pi$ may be also strengthened by the same two-step mechanism. Figures 5(a) and 5(b) show that the cross sections for capture into the $2\,^3\Sigma^-$ and $3\,^3\Sigma^-$ states are much smaller than those into the $2\,^3\Pi$ and $3\,^3\Pi$ states in the low-energy region. This can be attributed to the weaker couplings of the former as displayed in Figs. 2 and 3. For both the initial $1\,^3\Sigma^-$ and $1\,^3\Pi$ states, electron capture into the $1\,^3\Delta$ state is smaller than that into all the other states for the entire energy region considered and cross sections for capture into $1\,^3\Delta$ from $1\,^3\Sigma^-$ are nonzero. As there are no direct couplings between these two states, the transition $1\,^3\Sigma^- \rightarrow 1\,^3\Delta$ must occur by a two-step process: $1\,^3\Sigma^- \rightarrow 1\,^3\Pi$ followed by $1\,^3\Pi \rightarrow 1\,^3\Delta$, for example.

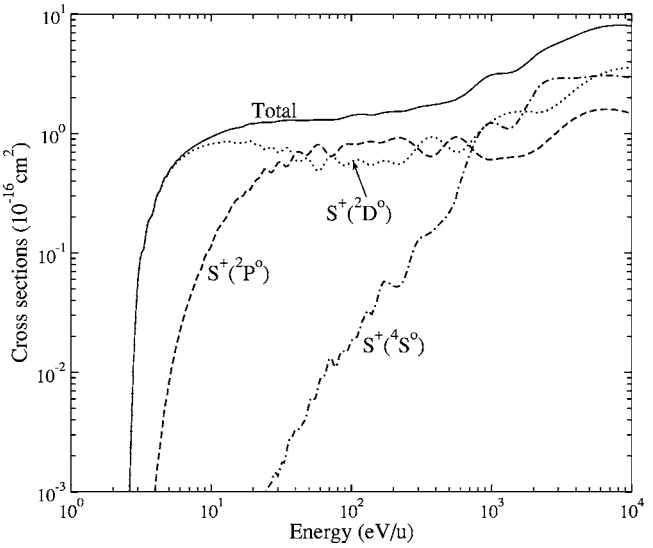

FIG. 6. Partial and total QMOCC charge-transfer cross sections due to $S^{2+}(^3P)$+He collisions as a function of relative collision energy E. *Total* denotes summation of cross sections for charge transfer into $S^+(^4S^0)$, $S^+(^2D^0)$, and $S^+(^2P^0)$.

Figure 6 displays and state-selective and total QMOCC cross sections. Below ~40 eV/u, the total charge-transfer cross sections are dominated by $S^{2+}(^3P)$+He$\rightarrow S^+(^2D^0)$+He^+, but capture into the $^2P^0$ states becomes comparable with that into the $^2D^0$ state with increasing energies. In the low-energy region, the contribution from the $^4S^0$ state is negligible, but above ~600 eV/u, charge transfer into the $^4S^0$ state begins to become significant. Table II lists state-selective and total rate coefficients obtained by averaging the quantal cross sections in Fig. 6 with a Maxwellian velecity distribation. The temperature ranges from 10 000 K to 5.0×10^6 K. For convenience, the rate coefficients are fitted to the form

TABLE II. Rate coefficients for electron capture into the $S^+(^4S^o, ^2D^o, ^2P^o)+He^+$ channels due to $S^{2+}(^3P)+He$ collisions. T is in 10 000 K and the rate coefficients are in cm^3/s. *Total* represents the rate coefficients summed over the exit channels.

T	$S^+(^4S^o)$	$S^+(^2D^o)$	$S^+(^2P^o)$	Total
1	1.23(−18)[a]	6.70(−16)	5.52(−19)	6.72(−16)
2	9.40(−18)	2.92(−13)	1.40(−15)	2.93(−13)
3	4.86(−17)	2.55(−12)	3.00(−14)	2.58(−12)
4	6.41(−16)	8.03(−12)	1.66(−13)	8.19(−12)
5	4.55(−15)	1.65(−11)	5.08(−13)	1.71(−11)
6	1.84(−14)	2.74(−11)	1.14(−12)	2.85(−11)
7	5.18(−14)	3.97(−11)	2.12(−12)	4.19(−11)
8	1.16(−13)	5.30(−11)	3.47(−12)	5.66(−11)
9	2.21(−13)	6.68(−11)	5.20(−12)	7.23(−11)
10	3.75(−13)	8.09(−11)	7.31(−12)	8.86(−11)
20	5.23(−12)	2.08(−10)	4.32(−11)	2.57(−10)
30	1.51(−11)	3.02(−10)	9.19(−11)	4.09(−10)
40	2.72(−11)	3.72(−10)	1.43(−10)	5.42(−10)
50	3.96(−11)	4.27(−10)	1.92(−10)	6.59(−10)
60	5.16(−11)	4.72(−10)	2.40(−10)	7.64(−10)
70	6.30(−11)	5.10(−10)	2.85(−10)	8.58(−10)
80	7.37(−11)	5.43(−10)	3.27(−10)	9.44(−10)
90	8.38(−11)	5.71(−10)	3.68(−10)	1.02(−09)
100	9.35(−11)	5.97(−10)	4.07(−10)	1.10(−09)
200	1.78(−10)	7.75(−10)	7.20(−10)	1.67(−09)
300	2.65(−10)	9.22(−10)	9.32(−10)	2.12(−09)
400	3.71(−10)	1.07(−09)	1.09(−09)	2.53(−09)
500	5.01(−10)	1.22(−09)	1.22(−09)	2.94(−09)

[a] $A(-B)=A\times10^{-B}$.

$$\alpha(T)=\sum_i a_i\left(\frac{T}{10\,000}\right)^{b_i}\exp\left(-\frac{T}{c_i}-\frac{\Delta E}{k_BT}\right), \qquad (12)$$

where α is the rate coefficient in cm^3/s, T is temperature in K, k_B is the Boltzmann constant, and ΔE is the experimental energy threshold in eV. The fitting parameters a_i (cm^3/s), b_i,

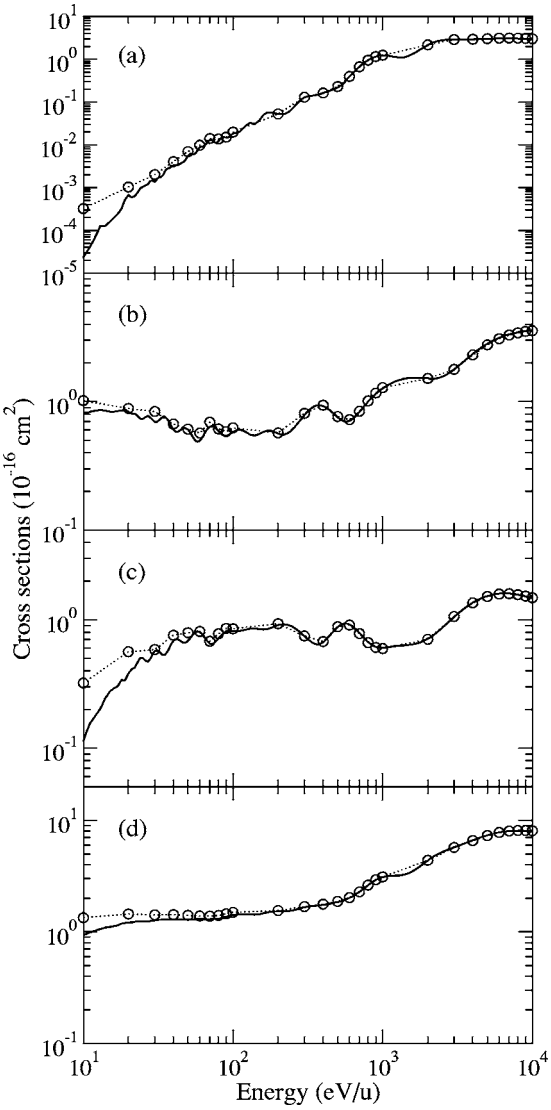

FIG. 7. Comparison of QMOCC and SCMOCC charge-transfer cross sections due to $S^{2+}+He$ collisions. Solid lines, QMOCC; ○, SCMOCC. (a), (b), and (c) represent charge transfer into the $S^+(^4S^0)+He^+$, $S^+(^2D^0)+He^+$, and $S^+(^2P^0)+He^+$ channels, while (d) corresponds to the total cross section.

TABLE III. Fitting parameters of rate coefficients for capture into $S^+(^4S^o, ^2D^o, ^2P^o)+He^+$ channels and the summed exit channels (Total). a_i and c_i are in units of cm^3/s and K, respectively.

Param.	$S^+(^4S^o)$	$S^+(^2D^o)$	$S^+(^2P^o)$	Total
a_1	7.90659(−14)[a]	9.67417(−11)	2.87970(−12)	4.25156(−11)
b_1	1.62413	3.96692(−01)	1.13458	7.22923(−01)
c_1	3.11532(+06)	−9.58658(+07)	4.76406(+06)	1.77887(+07)
a_2	−7.00086(−14)	−1.06442(−10)	−2.99598(−12)	−4.87251(−11)
b_2	1.89560	5.71057(−01)	1.28984	8.78844(−01)
c_2	1.48832(+05)	8.71444(+04)	1.29869(+05)	7.41017(+04)
ΔE	1.179	3.023	4.224	3.023

[a] $A(-B)=A\times10^{-B}$.

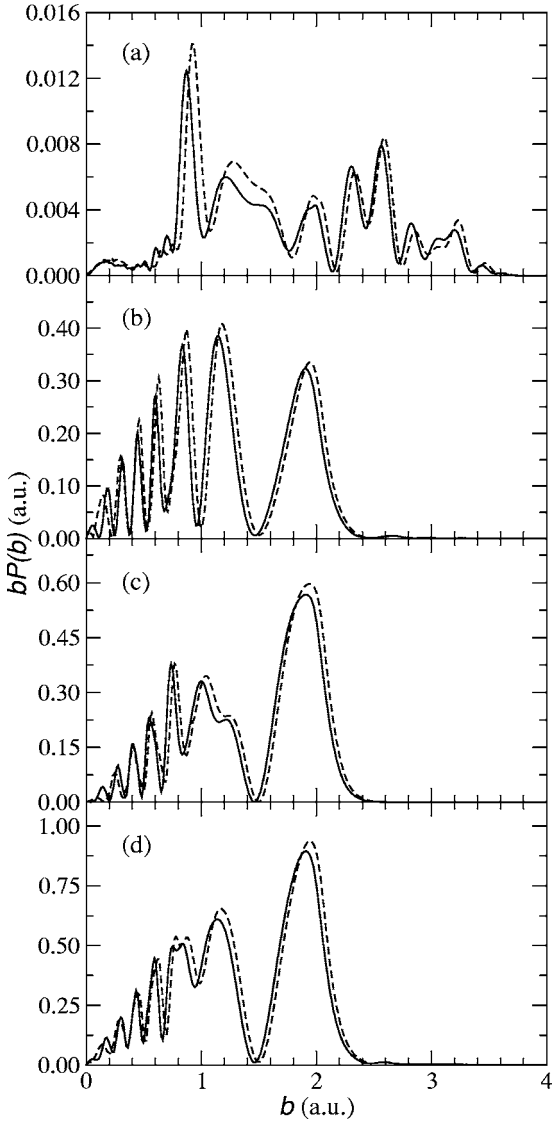

FIG. 8. Comparison of QMOCC and SCMOCC charge-transfer transition probabilities $P(b)$ times impact parameters b as a function of b at $E=100$ eV/u. Solid lines, QMOCC; dashed lines, SCMOCC. (a), (b), and (c) represent charge transfer into $S^+(^4S^0)+He^+$, $S^+(^2D^0)+He^+$, and $S^+(^2P^0)+He^+$ channels, while (d) corresponds to total charge transfer, a summation over the three final channels. In the quantal case, we take $b=J/k$.

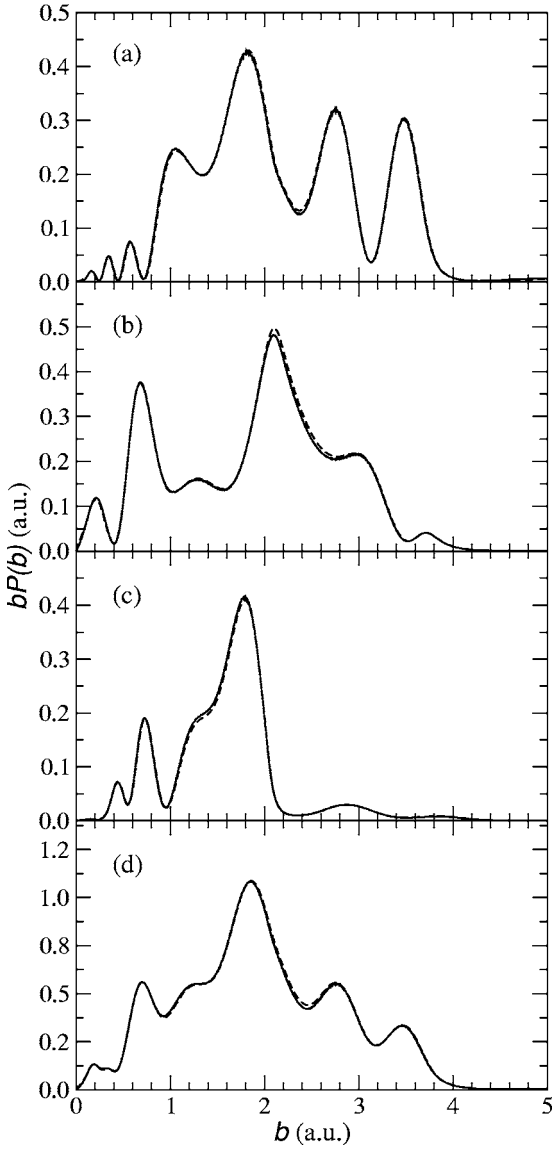

FIG. 9. Similar to Fig. 8 but $E=1.0$ keV/u.

and c_i (K) are given in Table III. The fits do not deviate from the computed rate coefficients by more than 7.1% for $20\,000 \leqslant T \leqslant 5.0\times10^6$ K, except for the capture into $^4S^0$ where the deviations are less than 31% for $T \geqslant 40\,000$ K.

In order to make a comparative study between quantal and semiclassical approaches, we performed semiclassical seven-channel close-coupling calculations for $S^{2+}+He$ collisions. The considered energy ranges from 10 eV/u to 10^4 eV/u. The results are plotted in Fig. 7 and are compared with the quantal cross sections. (a), (b), and (c) in Fig. 7 represent state-selective capture into $S^+(^4S^0)$, $S^+(^2D^0)$, and $S^+(^2P^0)$, while (d) corresponds to the total cross sections. It can be seen that for not only the total but also state-selective transitions, the QMOCC and SCMOCC cross sections are in excellent agreement except for the very-low-energy region (<40 eV/u). Below 40 eV/u, discrepancies between the QMOCC and SCMOCC cross sections increase with decreasing energies. These discrepancies may be caused by the limitation of semiclassical theory itself, which is invalid for lower energies. Furthermore, one finds that for the stronger transitions, the agreement between the quantal and semiclassical results is much better than that for the weaker transitions. For example, at 10 eV/u, the SCMOCC and QMOCC cross sections for capture into $S^+(^4S^0)$, $S^+(^2D^0)$, and $S^+(^2P^0)$ differ by one order of magnitude, 24%, and a factor of 2. The worse agreement may be related to the difficulty of treating weak transitions, which is a problem in all theoretical approaches. Accordingly, not only quantal scattering matrix elements but also semiclassical transition probabilities are probably of relatively large error. Fortunately capture into $S^+(^4S^0)$ is too small to contribute significantly to the total cross sections, as shown in Fig. 7(d). Castillo and Méndez [14] met similar difficulties when investigating

charge transfer for C^{2+}+He collisions. They found larger discrepancies for weak transitions, but excellent agreement for strong transitions, when comparing quantal and semiclassical cross sections.

The charge-transfer transition probabilities $P(b)$ times impact parameters b as a function of b are plotted at $E=100$ eV/u and 1 keV/u, respectively, in Figs. 8 and 9 to give a more detailed comparison of the quantal and semiclassical transition probabilities. (a), (b), and (c) display the state-selective $P(b)$ times b for capture into $^4S^0$, $^2D^0$, and $^2P^0$, while (d) corresponds to the total $P(b)$ times b. From Figs. 8 and 9, one sees good agreement between the quantal and semiclassical results for both the total and state-selective transition probabilities. In particular, at 1 keV/u, agreement is excellent. Figure 8 displays more violent oscillatory structures than Fig. 9. To check the change of oscillatory behavior with energies, we calculated transition probabilities at several more energies from 10 eV/u to 7 keV/u. It is found that the lower the energies are, the more violent the oscillation of $bP(b)$. This is because the oscillatory frequency is proporional to $1/\sqrt{E}$. The total $bP(b)$ in Figs. 8 and 9 reaches its peak magnitude of $\sim$0.9 a.u. and $\sim$1.1 a.u. at $b=1.95$ a.u. and weakens to 0.01 a.u. at $b=2.65$ a.u. and 4.16 a.u. This indicates that the contribution to the transition probabilities from large impact parameters, or high partial waves of angular momentum, increases with increasing energies.

V. SUMMARY

A comparative study of charge transfer in collisions of S^{2+} and helium has been made by using both the quantal and semiclassical molecular-orbital close-coupling approaches. We adopted the multireference single- and double-excitation configuration-interaction method to evaluate the molecular electronic structure and coupling matrix elements between the adiabatic molecular states for the SHe^{2+} system. Quantal and semiclassical cross sections are presented for electron capture into the $S^+(^4S^0, ^2D^0, ^2P^0)+He^+$ channels for collisions of $S^{2+}(^3P)$ with He^+ with relative collision energies between 2.5 eV/u and 10 keV/u. The state-selective and total cross section from the two approaches have been compared and good agreement has been found. The calculations show that at collision energies below about 40 eV/u, charge transfer is dominated by $S^{2+}(^3P)+He \rightarrow S^+(^2D^0)+He^+$, and capture into the $^2P^0$ and $^4S^0$ states becomes comparable with that into the $^2D^0$ state above 40 eV/u and 600 eV/u, respectively. Rate coefficients are given for temperatures between 10 000 K and 5.0×10^6 K. A detailed comparison of quantal and semiclassical transition probabilities has been discussed.

ACKNOWLEDGEMENTS

L.B.Z. and P.C.S. acknowledge support from NASA Grant No. NAG5-11453 and NSF Grant No. INT-0300708. R.J.B, J.P.G, and G.H. acknowledge financial support from Deutsche Forschungsgemeinschaft Grant No. Bu 450/7-3 and the Fonds der Chemischen Industrie. M.K. acknowledges support from the Ministry of Education, Science, Sport, Culture and Technology, Japan Society for Promotion of Science (JSPS) for the US-JP Collaborative Research Program, and Collaborative Research Grant by National Institute for Fusion Science.

[1] C. M. Lisse, D. J. Christian, K. Dennerl, K. J. Meech, R. Petre, H. A. Weaver, and S. J. Wolk, Science **292**, 1343 (2001).
[2] F. P. Keenan, C. A. Ramsbottom, K. L. Bell, a. A. Berrington, A. Hibbert, W. A. Feibelman, and W. P. Blair, Astrophys. J. **438**, 500 (1995).
[3] A. D. Silber, S. F. Anderson, B. Margon, and R. A. Downers, Astrophys. J. **462**, 428 (1996).
[4] Anh-Thu Le, C. D. Lin, L. F. Errea, L. Méndez, A. Riera, and B. Pons, Phys. Rev. A **69**, 062703 (2004).
[5] L. F. Errea, C. Harel, H. Jouin, L. Méndez, B. Pons, and A. Riera, J. Phys. B **31**, 3527 (1998).
[6] M. Kimura and N. F. Lane, Adv. At., Mol., Opt. Phys. **26**, 79 (1990).
[7] H. Shang, A. E. Glassgold, F. H. Shu, and S. Lizano, Astrophys. J. **564**, 853 (2002).
[8] D. E. Osterbrock, H. D. Tran, and S. Veilleux, Astrophys. J. **389**, 305 (1992).
[9] D. E. Osterbrock, H. D. Tran, and S. Veilleux, Astrophys. J. **389**, 196 (1992).
[10] F. P. Keenan, L. H. Aller, K. L. Bell, S. Hyung, F. C. McKenna, and C. A. Ramsbottom, Mon. Not. R. Astron. Soc. **281**, 1073 (1996).
[11] J. Caillat, A. Dubois, I. Sundvor, and J.-P. Hansen, Phys. Rev. A **70**, 032715 (2004).
[12] L. B. Zhao, P. C. Stancil, H. P. Liebermann, P. Funke, and R. J. Buenker, Phys. Rev. A **71**, 060701(R) (2005).
[13] C. Y. Lin, P. C. Stancil, J.-P. Gu, R. J. Buenker, and M. Kimura, Phys. Rev. A **71**, 062708 (2005).
[14] J. F. Castillo and L. Méndez, Phys. Rev. A **56**, 421 (1997).
[15] L. B. Zhao, P. C. Stancil, J.-P. Gu, H.-P. Liebermann, P. Funke, R. J. Buenker, and M. Kimura, Phys. Rev. A **71**, 062713 (2005).
[16] R. J. Buenker and S. D. Peyerimhoff, Theor. Chim. Acta **35**, 33 (1974); **39**, 217 (1975).
[17] R. J. Buenker, in *Current Aspects of Quantum Chemistry*, Vol. 21 of *Studies in Physical and Theoretical Chemistry*, edited by R. Carbo (Elsevier, Amsterdam, 1981), p. 17.
[18] S. Krebs and R. J. Buenker, J. Chem. Phys. **103**, 5613 (1995).
[19] M. Kimura, J. P. Gu, H. P. Liebermann, Y. Li, G. Hirsch, R. J. Buenker, and A. Dalgarno, Phys. Rev. A **50**, 4854 (1994).
[20] K. Amezian and M. C. Bacchus-Montabonel, Chem. Phys. Lett. **199**, 487 (1992).
[21] S. Bashkin and J. O. Stoner, *Atomic Energy Levels and Grotrian Diagrams* (North-Holland, Amesterdam, 1975).
[22] NIST Atomic Spectra Database, website http://physics.nist.gov/asd
[23] B. Zygelman, D. L. Cooper, M. J. Ford, A. Dalgarno, J. Gerratt, and M. Raimondi, Phys. Rev. A **46**, 3846 (1992).

[24] B. H. Bransden and M. R. C. McDowell, *Charge Exchange and the Theory of Ion-Atom Collisions* (Clarendon Press, Oxford, 1992).
[25] A. R. Turner, D. L. Cooper, J. G. Wang, and P. C. Stancil, Phys. Rev. A **68**, 012704 (2003).
[26] B. R. Johnson, J. Comput. Phys. **13**, 445 (1973).
[27] R. K. Janev, L. P. Presnyakov, and V. P. Shevelko, *Physics of Highly Charged Ions* (Springer-Verlag, New York, 1985).
[28] L. F. Errea, C. Harel, H. Jouin, L. Méndez, B. Pons, and A. Riera, J. Phys. B **27**, 3603 (1994).
[29] M. Kimura, H. Sato, and R. E. Olson, Phys. Rev. A **28**, 2085 (1983).